



Dual-porosity model of mass transport in electroporated biological tissue: Simulations and experimental work for model validation



Samo Mahnič-Kalamiza^{a,b,*}, Damijan Miklavčič^b, Eugène Vorobiev^a

^a Centre de Recherches de Royallieu-BP 20529, University of Technology of Compiègne, 60205 Compiègne Cedex, France

^b Faculty of Electrical Engineering, University of Ljubljana, Tržaška c. 25, SI-1000 Ljubljana, Slovenia

ARTICLE INFO

Article history:

Received 23 June 2014

Revised 22 September 2014

Accepted 23 September 2014

Available online 30 October 2014

Editor Proof Receive Date 30 October 2014

Keywords:

Electroporation

Pulsed electric fields

Mass transfer

Diffusion

Pressing

Mathematical modeling

ABSTRACT

Electroporation or pulsed electric field treatment is an important technique for facilitating mass transport in biological tissues with proven benefits for the food processing industry. One of the challenges in understanding its basic mechanisms and effects is mass transport processes in treated tissue. We recently presented a mathematical model called dual-porosity model to describe post-electroporation diffusion in biological tissue and filtration–consolidation behavior of electroporated tissue during pressing. In this work we bring the two analogues together and study the model's applicability and performance by comparing experimental and simulated kinetics. We use two kinds of plant tissue of dissimilar properties (sugar beet taproot and apple fruit), but employ the same methodology to evaluate the validity of basic assumptions. We show that the model describes experimental data and provides more insight into the mass transport processes during post-pulse extraction/pressing. We comment on treatment conditions that expose limitations and indicate possibilities for future development.

Industrial relevance: In order to study and optimize extraction processes following treatment of biological material with electroporation (pulsed electric fields), good knowledge on mass transport processes in electroporated tissue is of essential importance. Development, final form and application of a new mathematical model are presented that will aid in understanding of mass transport by solute diffusion and filtration–consolidation behavior of electroporated tissue under external pressure. It is foreseen that such a model could be used for predictive purposes and optimization of treatment parameters in industrial applications of electroporation, where *in silico* modeling can thus help find new or improved protocols to increase efficiency and efficacy in pulsed electric field applications.

© 2014 Elsevier Ltd. All rights reserved.

1. Introduction

The terms electroporation, electropermeabilization, and pulsed electric field treatment, are commonly used to refer to the application of short, high-intensity electrical impulses to biological material and consequences that such electric pulses have on biological material (Kotnik, Kramar, Pucihar, Miklavcic, & Tarek, 2012; Raso & Heinz, 2010; Yarmush, Golberg, Serša, Kotnik, & Miklavčič, 2014). We prefer to and will use the term electroporation throughout the remainder of this article. In electroporation, the electric pulses of specific parameters are applied to the target tissue or cell suspension, the parameters depending on the intended goal of application. Often the objectives

are to induce a transient increase in cell membrane permeability (Gehl, 2003; Haberl, Miklavcic, Sersa, Frey, & Rubinsky, 2013; Marty et al., 2006; Zorec, Prät, Miklavčič, & Pavšelj, 2013), or to permanently damage and ultimately destroy the cells (Goettel, Eing, Gusbeth, Straessner, & Frey, 2013; Golberg & Yarmush, 2013; Jiang, Qin, & Bischof, 2014; Morales-de la Pena, Elez-Martinez, & Martin-Belloso, 2011; Saulis, 2010). To achieve selective extraction of bio-compounds, complete destruction of the cells is an undesirable effect leading to impure solutions.

A closer look at the electroporation processes on the biochemical level reveals that treatment outcome and efficacy are largely governed by electrical and (related) chemical properties of the treated material, and mass transport that occurs during and after application of electric pulses (Kotnik et al., 2012; Li & Lin, 2011a; Li, Tan, Yu, & Lin, 2013b; Pucihar, Kotnik, Miklavcic, & Teissie, 2008; Sel et al., 2005). These properties and transport phenomena influence the development of the electropermeabilized state of the cell membrane during electroporation, and continue to be important in the post-pulsation period of pore shrinkage, resealing, cell lysis, etc. (Reigada, 2014; Sridhara & Joshi, 2014).

* Corresponding author at: Université de Technologie de Compiègne (UTC), Département de Génie des Procédés Industriels, Laboratoire Transformations Intégrées de la Matière Renouvelable, Centre de Recherches de Royallieu-BP 20529, 60205 Compiègne Cedex, France. Tel.: +33 6 52 17 30 92.

E-mail addresses: samo.mahnic@utc.fr, samo.mahnic@fe.uni-lj.si, samo.mahnic@gmail.com (S. Mahnič-Kalamiza).

Mass transport is also of significance in light of the intended purpose of electroporation treatment application. If electroporation is applied to facilitate solute extraction by diffusion (increasing rate, yield, etc.) or to change the permeability of the cell membrane and overall tissue for improving juice expression or tissue dehydration, the mass transport processes (both of solutes and liquid) are of primary importance and should be the focus of study. Moreover, since much the same processes of transport in electroporated cells and tissues are of interest in other fields of electroporation applications, such as biomedicine—in e.g. electrochemotherapy (Cadossi, Ronchetti, & Cadossi, 2014; Miklavcic, Mali, Kos, Heller, & Sersa, 2014), gene transfection (Dean, 2013), trans- and intradermal drug delivery (Becker, 2012), etc.—the study of mass transport phenomena in electroporated biological material is a trans-domain research field. Within this expanded field incorporating biology, medicine, pharmacology, electrical engineering, process and food engineering, chemistry and chemical physics, as well as several other domains, there is an abundance of published theoretical and experimental approaches employed to identify and describe the basic mechanisms of electroporation. These developments and theoretical advances add pieces to the greater puzzle that is the theory of electroporation. Mass transport phenomena represent an important integral part of this work in progress. The significance of the trans-domain span in research on electroporation is in the analogies that appear throughout the various domains of electroporation applications that can complement to form a more complete and complex picture of the effects of short-duration, high-intensity electric fields on biological material. To illustrate with a particular example; if passive diffusion of solute through an electroporated membrane is the predominant mechanism of mass transport in electroporated tissue in the post-pulse period (Pucihar et al., 2008), a study of the process is of greatest importance to biomedicine in e.g. electrochemotherapy (introduction of molecules of a chemotherapeutic drug into tumor cells—see sources on electrochemotherapy cited above), and for food processing industry in e.g. industrial extraction of valuable compounds from their primary biological sources (extraction of carbohydrates, polyphenols, lipids, etc.) (see e.g. Boussetta, Soichi, Lanoiselle, & Vorobiev, 2014; Donsi, Ferrari, & Pataro, 2010; Grimi et al., 2014; Liu, Lebovka, & Vorobiev, 2013). To give another example; liquid pressure gradients are present in many of the tissues which are of interest in electroporation. Plant cells for instance maintain their shape and plant tissue its turgidity due to turgor pressure, resulting from a solute concentration imbalance across the cell membrane that causes an osmotic pressure build-up (Campbell et al., 2008; Pereira, Galindo, Vicente, & Dejmeek, 2009). In tumors, poorly formed vascular system and lacking lymphatic drainage system result in local gradients in interstitial fluid pressure, leading to a higher intratumoral pressure as compared to liquid pressure in the surrounding healthy tissue (Ariffin, Forde, Jahangeer, Soden, & Hinchion, 2014; Liu, Brown, Ewing, & Schlesinger, 2011; Pusenjak & Miklavcic, 2000; Simonsen, Gaustad, Leinaas, & Rofstad, 2012). Rendering the cell membrane semipermeable in presence of pressure gradients will, in theory, result in filtration flows in the direction opposite to that of the pressure gradient both during and after electroporation. Pressure gradients exist in untreated tissue (e.g. osmotic pressure, interstitial fluid pressure) that may be of significant importance already during application of electric pulses, and after electroporation treatment, a pressure gradient is established by the externally-applied pressure during the pressing stage. This is yet another mechanism of solid–liquid mass transport of importance in relation to electroporation in two disparate domains of electroporation application. If the same approach, from the theoretical point of view, can be used to study two very disparate goals of electroporation application, one should need to develop mathematical descriptions of the process physics (i.e. *models*) once only for the process and then apply them, with necessary modifications, to each particular application. Following this paradigm, we recently published two works on the development of a mathematical model we refer to as the dual-porosity model. The first account presents the

model as describing extraction or introduction of solute by diffusion out of or into electroporated biological tissue (Mahnič-Kalamiza, Miklavcic, & Vorobiev, 2014). We used sucrose extraction from sugar beets for the model study, but also suggested two possible applications of the model for introduction of compounds into animal or plant cells. Furthermore, the analogy between diffusion and liquid flow laws allows for a rapid adaptation of the model for the problem of filtration–consolidation behavior of electroporated tissue, and is the subject of the second account (Mahnič-Kalamiza & Vorobiev, 2014). In the present work, we bring the two analogues together and examine the model validity and its performance by comparing experimental data with diffusion/expression kinetics, which result from simulations done using the model proposed. We use two kinds of vegetable tissue as model material with markedly different properties (sugar beet taproot and apple fruit), but employ the same methodology to determine if the postulates and simplifications during model development are justifiable, i.e. can results of model simulations be reconciled with those obtained via experiments. We also show under what treatment conditions it is expected the model will be insufficient to describe experimental kinetics, since the model has been simplified in order to preserve the ability to work with its analytical solution. This analysis enables us to indicate how the model needs to be expanded and to point towards the possible improvements that will need to be accomplished during future development.

2. Materials and methods

2.1. Disintegration index Z

The disintegration index Z is a conductivity-based measure that can be used to estimate the degree of tissue damage during or after treatment—in our case electrical—and is defined as $Z = (\sigma - \sigma_i) / (\sigma_d - \sigma_i)$, where σ is the material conductivity (during or at the end of treatment protocol application), σ_i is the conductivity of the intact sample tissue (prior to treatment), and σ_d corresponds to the conductivity of a tissue sample considered to be destroyed by the treatment, i.e. fully treated. The value of Z increases during electrical treatment, beginning at 0 (intact tissue) and approaches 1 (completely permeabilized cells—i.e. maximally damaged tissue) as the conductivity of the treated sample increases. Various methods can be used to determine σ_d ; e.g. freezing–thawing or high-intensity long-duration electroporation have been proposed (Vorobiev & Lebovka, 2008). For the purposes of the present study, an average σ_d was obtained by averaging the measured conductivity of several tissue samples, each of which was treated with 50 trains of 10 pulses of amplitude 400 V (per 5 mm electrode distance), pulse width 100 μ s and 5 s pause in between the trains to allow for cooling of the sample and thus avoiding thermal damage to the tissue.

2.2. Diffusion experiments

Cylindrical samples (disks) of sugar beet taproot and apple fruit tissue (skin removed) were obtained from 5 mm thick sugar beet taproot or apple fruit slices.¹ All samples measured 25 mm in diameter. Each sample was subjected to electroporation treatment by applying 150, 200, 300, or 400 V between two parallel plate stainless-steel electrodes at 5 mm inter-electrode distance (sample thickness). Our intent was to subject the treated tissue to field strengths of 300, 400, 600, and 800 V/cm, respectively. Note that this would hold if the tissue were electrically homogeneous material, and only in the central area away from electrode edges. Rectangular pulses of alternating polarity (see Fig. 2) of 100 μ s duration each, and pulse repetition frequency of 1 kHz, were delivered within each train of eight pulses. Two such trains

¹ In the remainder of the paper, for brevity, we refer to «apple fruit tissue» and «sugar beet taproot tissue» as «apple tissue» and «sugar beet tissue», respectively.

were delivered with a pause of 1 s between the two trains. This protocol will here on be referred to as Protocol A (see Fig. 2a). The pulses were provided by a custom-built pulse generator with peak output current of 38 A at the maximum attainable voltage of 400 V, assembled by Service Electronique UTC, Compiègne, France.

The samples were then removed from the treatment chamber, after which the surfaces of the sample disks were put into contact with absorbent paper and thus the surfaces dried, in order to remove the sugary liquid. This liquid is present due to cutting and possibly due to electro-osmotic or pressure-change effects that occur during the electroporation treatment. Note that had the surfaces not been dried, the juice on the surface would cause an immediate increase in the sugar concentration in the solution at the beginning of the experiment, resulting in kinetics also known as the “washing stage” of the process (El Belghiti & Vorobiev, 2004). This effect is not captured by the model, neither is it easy to subtract it from the kinetics due to varying juice sugar concentration and amount of this surface liquid that varies per sample. The surface-dried samples were placed into a flask with a magnetic stirrer. The sample-containing liquid was constantly agitated and sampled at regular intervals; total soluble solids (i.e. predominantly sugar) concentration was analyzed with a digital refractometer. The liquid-to-solid ratio was 2:1 in all experiments.

The quantity which is measured by the digital refractometer is sugar (more precisely total soluble solids) concentration in liquid with unit degrees Brix ($^{\circ}\text{Bx}$), where 1 $^{\circ}\text{Bx}$ is 1 g of sucrose in 100 g of solution and represents the concentration of the solution as percentage by weight (% w/w). We know the initial sugar content of the aqueous solution $^{\circ}\text{Bx}_0$ (normally equal to zero), we measure and record (during experiment) the current sugar content $^{\circ}\text{Bx}(t)$ —i.e. the extraction kinetics, and the final sugar concentration $^{\circ}\text{Bx}_d$ can be determined separately. Theoretically, $^{\circ}\text{Bx}_d$ is the total solute concentration in solution in ideal conditions of completely permeabilized tissue and after infinite time of diffusion. In practice, it is easily determined by measuring the solute concentration in pure fruit/root juice, and scaling the measurement according to the extracting liquid/juice mass ratio (also known as the solid–liquid ratio). Since initial and maximum concentrations are known, we can define and calculate *normalized degree Brix* at time t —i.e. $B(t)$, as

$$B(t) = \frac{{}^{\circ}\text{Bx}(t) - {}^{\circ}\text{Bx}_0}{{}^{\circ}\text{Bx}_d - {}^{\circ}\text{Bx}_0}. \quad (1)$$

We use Normalized Brix throughout the remainder of this paper as a measure for the amount of solute (e.g. sugar) that has diffused out of the tissue sample in time t . It takes the values from the interval $0 \leq B(t) \leq 1$, and is dimensionless. It can be calculated from measurements with the refractometer, according to Eq. (1). The schematic illustration of the diffusion experiment is given by Fig. 1.

2.3. Pressing experiments

We used cylindrical samples of sugar beet and apple tissue, 25 mm in diameter and of 5 mm thickness. The samples were placed between two parallel plate stainless-steel electrodes, and electroporation pulses were applied using three different protocols (see Fig. 2). Protocol A: The voltage was varied, using 150 V, 200 V, 300 V, 350 V, or 400 V applied to the electrodes. Pulses of alternating polarity were delivered in two trains of eight pulses per train, with repetition frequency of 1 kHz within the train, 1 s pause between the two trains, and 100 μs pulse duration. Protocol B: The voltage was again varied as in Protocol A, however only two unipolar pulses were delivered of 800 μs each, and with a time delay of 1 s in between the two pulses. Protocol C: The voltage was varied as in Protocol A and Protocol B, and eight pulses of singular polarity were delivered, 100 μs in duration each second (i.e. at pulse repetition frequency of 1 Hz). This protocol is also known as one of the *standard protocols for electrochemotherapy* (Marty et al., 2006). Note that the total treatment time t_t (product of pulse duration t_p , number of pulses n_p and number of trains n_t) as calculated from the pulsing protocol was the same for Protocols A and B ($t_t = 1.6$ ms), and was 50% lower in case of Protocol C ($t_t = 0.8$ ms) as compared to the two other protocols. The delivered energy in our setup as calculated from the measured current falls between 6 J/kg (minimum attained for sugar beet, Protocol C, 150 V) and 250 J/kg (maximum attained for apples, Protocol B, 400 V). In terms of delivered energy and treatment time, these treatment protocols are normally not encountered in food processing, where energies on the order of several kJ/kg are commonly delivered to target tissues (Donsi et al., 2010; Turk, Vorobiev, & Baron, 2012). The maximum total delivered energy on the order of 0.25 kJ/kg results—in worst case, i.e. not accounting for any heat dissipation via electrodes or treatment chamber surfaces—in a negligible increase in sample temperature by less than 0.1 K. This estimate is based on the thermal capacity of apple tissue, found in Mykhailiyk and Lebovka

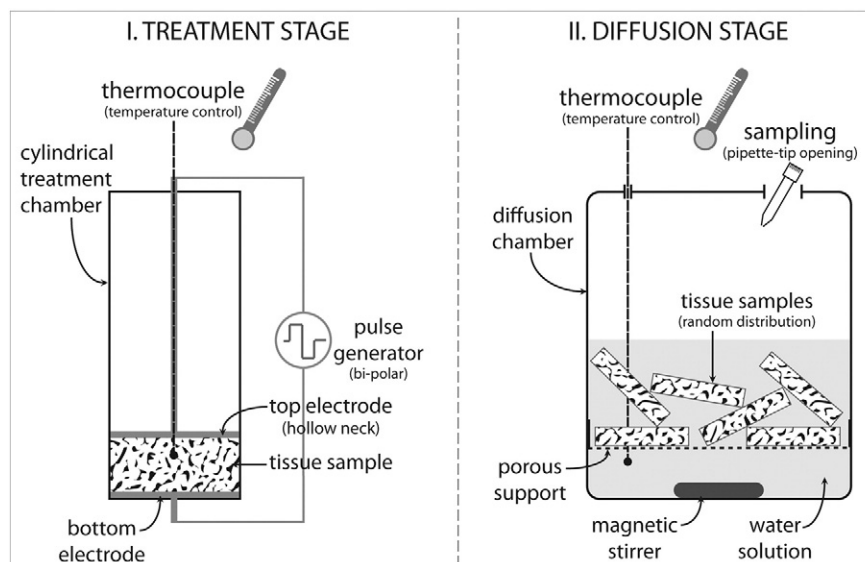


Fig. 1. Schematic representation of the diffusion experiment setup—electroporation treatment (left) and subsequent diffusion (right).

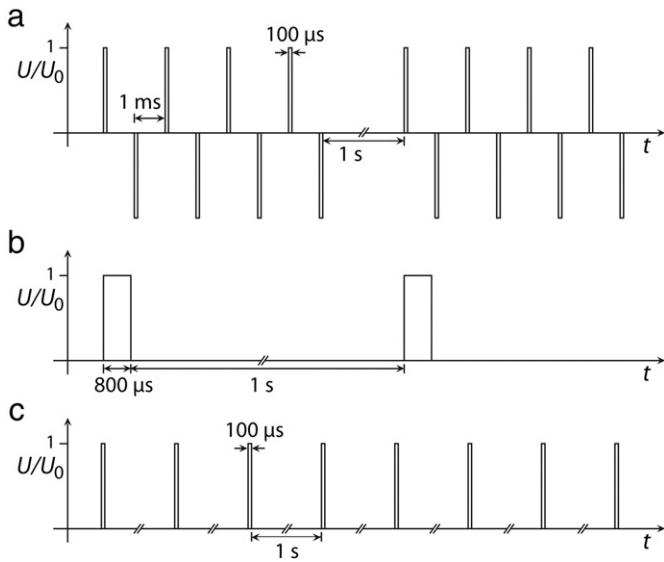


Fig. 2. Schematic representation of the three pulse delivery protocols: Protocol A (a), Protocol B (b), and Protocol C (c). Pulse widths and distances are to scale, except where denoted otherwise—the ‘//’ sign indicates a break in the axis (i.e. there is a 1 s long pause between every two pulses in between which the axis brake is indicated).

(2014), and known maximum energy that was delivered. We further discuss the reasons for and implications of our particular choice of low-intensity, “gentler” treatment protocols in Section 3.

In all cases, regardless of the electroporation protocol, the electric treatment was followed by pressing. Electroporated samples were immediately placed into a specially fabricated treatment chamber and subjected to a load of 150 N—about 580 kPa (apple), or 300 N—about 290 kPa (sugar beet), using a texturometer. The piston displacement was recorded by the texturometer under constant pressure (force) application during 1 h.

Piston displacement equals the sample deformation along the axis of the pressure application. At the end of Section 2.5 on the dual-porosity model for filtration–consolidation, we show how the simulated pressure distribution in sample in time can be related with the measured deformation. This is necessary in order to enable comparison of experimental and model results.

2.4. The dual-porosity model of solute diffusion

The dual-porosity approach for studying diffusion of solute in electroporated tissue is presented in detail in Mahnič-Kalamiza et al. (2014). Here, we give the experimental setup geometry (Fig. 3), the partial differential equation system (Eqs. (2)–(3)) that represents the fundamental model equations for diffusion according to the dual-porosity model, the appropriate boundary and initial conditions (Eq. (4)–(9)) and the final solution (Eqs. (10)–(14)) of the system. All but Fig. 3 are reproduced from Mahnič-Kalamiza et al. (2014).

The fundamental model equations for the extracellular and the intracellular phase (space) are, respectively,

$$\frac{\partial c_e(z, t)}{\partial t} - D_{s,e} \frac{\partial^2 c_e(z, t)}{\partial z^2} - \frac{1-\varepsilon}{\varepsilon} k \cdot [c_i(z, t) - c_e(z, t)] = 0 \quad (2)$$

$$\frac{\partial c_i(z, t)}{\partial t} + k \cdot [c_i(z, t) - c_e(z, t)] = 0 \quad (3)$$

where c_e and c_i are extracellular and intracellular solute concentrations, respectively, $D_{s,e}$ is the intrinsic diffusion coefficient of solute species s in extracellular space, ε is the tissue porosity (cell-to-extracellular volume ratio, i.e. $\varepsilon = 1 - F$, where F is cell volumetric fraction), and k is the transmembrane flow coefficient defined by Eq. (15).

The boundary conditions (BC) are determined, in summary, as follows; the left BC requires the extracellular concentration of solute be 0 for all times, since we are working under the supposition of infinite dilution outside the tissue sample,

$$c_e(t)|_{z=h/2} = 0. \quad (4)$$

The intracellular concentration at that boundary is seemingly undetermined, but can be expressed by combining Eq. (3) with the left BC for extracellular space (Eq. (4)), solving the resulting ordinary differential equation yields

$$c_i(t)|_{z=h/2} = c_{i0} e^{-kt}. \quad (5)$$

The right boundary is the plane of symmetry—the central plane of the tissue sample perpendicular to the principal axis of diffusion (see Fig. 3). At this plane of symmetry, Fick’s diffusive flux must equal zero

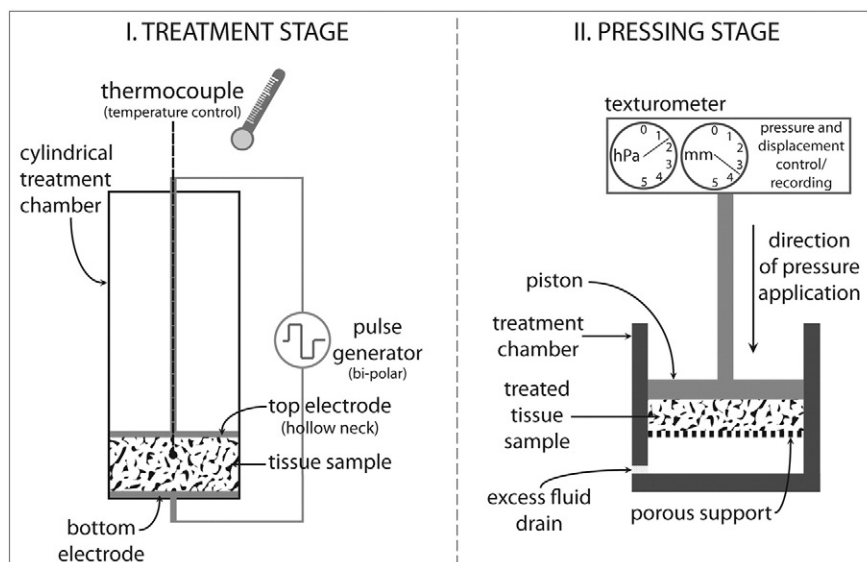


Fig. 3. Schematic representation of the pressing experiment setup—electroporation treatment (left) and subsequent pressing (right).

for both the intra- and the extracellular phase, as there are no solute sources or sinks (absence of chemical reactions). We have

$$\left. \frac{\partial c_e(t)}{\partial z} \right|_{z=0} = 0 \quad (6)$$

$$\left. \frac{\partial c_i(t)}{\partial z} \right|_{z=0} = 0. \quad (7)$$

For the initial conditions (IC) we suppose a homogeneous initial distribution of solute concentrations. The initial concentrations need not be equal in the extracellular and intracellular space, which is a valid assumption for intact or poorly permeabilized tissue where solute remains intracellular. We define constants c_{e0} and c_{i0} as

$$c_e(z, 0) = c_{e0} \quad (8)$$

$$c_i(z, 0) = c_{i0}. \quad (9)$$

The solution of the system of partial differential equations (Eqs. (2)–(3)) for BC and IC (Eqs. (4)–(9)) is

$$c_e(z, t) = \frac{4c_{i0}}{\pi} \sum_{n=0}^{\infty} \frac{(-1)^n}{2n+1} \cos(\lambda_n z) \left(C_{n,1} e^{\gamma_{n,1} t} \left(\frac{\gamma_{n,1}}{k} + 1 \right) + C_{n,2} e^{\gamma_{n,2} t} \left(\frac{\gamma_{n,2}}{k} + 1 \right) \right), \quad (10)$$

$$c_i(z, t) = \frac{4c_{i0}}{\pi} \sum_{n=0}^{\infty} \frac{(-1)^n}{2n+1} \cos(\lambda_n z) \left(C_{n,1} e^{\gamma_{n,1} t} + C_{n,2} e^{\gamma_{n,2} t} - e^{-kt} \right) + c_{i0} e^{-kt}, \quad (11)$$

where

$$C_{n,1} = \frac{\left(\frac{c_{e0}}{c_{i0}} - 1 \right) k - \gamma_{n,2}}{\gamma_{n,1} - \gamma_{n,2}}, \quad (12)$$

$$C_{n,2} = \frac{\left(1 - \frac{c_{e0}}{c_{i0}} \right) k + \gamma_{n,1}}{\gamma_{n,1} - \gamma_{n,2}}, \quad (13)$$

and

$$\gamma_{n,1,2} = \frac{-((\delta + 1)k + \lambda_n^2 D_{s,e}) \pm \sqrt{((\delta + 1)k + \lambda_n^2 D_{s,e})^2 - 4k\lambda_n^2 D_{s,e}}}{2}, \quad (14)$$

where for the sake of algebra we have set $\delta = (1 - \varepsilon)/\varepsilon$. The eigenvalues λ_n equal $\lambda_n = (2n + 1) \cdot \pi/h$.

The transmembrane flow coefficient (also termed mass transfer coefficient) k is the critical constituent of the model capturing the electroporation effects on the cell membrane. If cells can be modeled as perfect spheres of radius R and membrane thickness d_m , $D_{s,0}$ is the solute diffusion rate in water at a given temperature, y_s is the pore diffusion hindrance coefficient and f_p is the stable pore surface fraction ($f_p = N_p \cdot A_p/A_0$, where N_p is the number of pores per cell, A_p is the average single pore area and A_0 is the cell area equaling $4\pi R^2$), we can determine k as

$$k = \frac{3D_{s,0}y_s f_p}{d_m R} \quad (15)$$

The electroporation treatment affects the pore surface fraction f_p as well as the hindrance coefficient y_s , assuming the radius of an average stable pore is dependent on treatment parameters. For more details on the hindrance coefficient and k , see Mahnič-Kalamiza et al. (2014).

2.5. The dual-porosity model of filtration–consolidation under external pressure

There is an obvious analogy from the mathematics and physics point of view between the Fick's law of diffusion and Darcy's law of liquid flow in porous media. The dual-porosity model as given by Eqs. (2)–(3) can therefore also be written to describe filtration–consolidation behavior of tissue under applied pressure, the model formulation remaining much the same, except for some replacements, omissions and added details. Namely, the diffusion rate $D_{s,e}$ is replaced by the hydraulic permeability k_e of the tissue over viscosity μ , i.e. k_e/μ , and the mass transport coefficient k by a similar proportionality coefficient α over viscosity, i.e. α/μ . We account for the initial tissue porosity ε already by permeability k_e and compressibility modulus $G_{e,e}$ that are not intrinsic, but rather quantities volume-averaged throughout the whole sample (for explanation see Section 3.2.1.1 in De Monte, Pontrelli, & Becker, 2013), and thus we drop the factor $(1 - \varepsilon)/\varepsilon$. And finally, the concentration gradients are replaced, as the driving forces of the transport processes, by the liquid pressure gradients, and thus concentrations c_e and c_i are replaced by liquid pressures p_e and p_i . We have, as analogues to the diffusion fundamental model equations (Eqs. (2)–(3)), the following equations

$$\frac{1}{G_{e,e}} \frac{\partial p_e}{\partial t} - \frac{\partial}{\partial z} \left(\frac{k_e}{\mu} \frac{\partial p_e}{\partial z} \right) - \frac{\alpha}{\mu} (p_i - p_e) = 0 \quad (16)$$

$$\frac{1}{G_{e,i}} \frac{\partial p_i}{\partial t} + \frac{\alpha}{\mu} (p_i - p_e) = 0. \quad (17)$$

These equations are, as in the diffusion problem, derived from the law of mass conservation. However, as opposed to solute concentration, which is both the measured/observed quantity and (via its gradient) the originating force for the diffusive solute flow, the liquid pressure though a driving force is not itself a subject of the mass conservation law. It has to be related to the conserved density and, consequently, the porosity of the respective phases by the *compressibility moduli*. More details on this can be found in Mahnič-Kalamiza and Vorobiev (2014). Compressibility modulus or its inverse, the bulk modulus, is traditionally defined as a relative change in volume (or void ratio) in response to a given pressure change. If void ratio e denotes the ratio between the void (liquid) and solid phase within the intra- and extracellular space, compressibility moduli can be determined from

$$\frac{\partial e_e}{\partial t} = - \frac{\partial p_e}{\partial t} \cdot \frac{\partial e_e}{\partial p_{e,S}} = \frac{1}{G_e} \frac{\partial p_e}{\partial t} \quad (18)$$

$$\frac{\partial e_i}{\partial t} = - \frac{\partial p_i}{\partial t} \cdot \frac{\partial e_i}{\partial p_{i,S}} = \frac{1}{G_i} \frac{\partial p_i}{\partial t}. \quad (19)$$

The bulk moduli G_e and G_i relate the change in void ratio with the loss of liquid pressure. In experiments we measure piston displacement and thus tissue sample deformation, and this measured deformation is more closely related to porosity (void to total volume ratio) than to the void ratio itself. For this reason, we have redefined the bulk moduli via averaged porosity of each space, so that

$$\bar{G}_{e,e} = G_e (1 + \bar{e}_e)^2 \quad (20)$$

$$\bar{G}_{e,i} = G_i(1 + \bar{\epsilon}_i)^2. \quad (21)$$

Note that in all but Eqs. (20)–(21), we omit the notation for averaged values. This definition makes initial estimates for the moduli readily obtainable from total- or end-deformation points reached in experiments. However, there is a trade-off. Averaging the void ratio, a function of both space and time, and assuming it constant, narrows down the generality of the model. It is now valid for a particular segment of the parameter space that demands the piston displacement be small as compared to the thickness of the entire sample. This condition is met if the tissue is not severely damaged by the applied treatment, something we have to keep in mind when interpreting model results. A more general approach omitting these simplifications is highly demanding in mathematical terms and unwieldy for analytical treatment (Petryk & Vorobiev, 2013).

To solve the system of Eqs. (16)–(17), we need appropriate boundary and initial conditions. The initial conditions can be rewritten from Eqs. (8)–(9) by simple replacement of concentration with liquid pressure, obtaining

$$p_e(z, 0) = p_{e0} \quad (22)$$

$$p_i(z, 0) = p_{i0}. \quad (23)$$

On the other hand, the boundary conditions are somewhat different. There is no central plane of symmetry in the mid-section of the tissue sample (see Fig. 4). Instead, we have a no-flux boundary at the sample–piston contact surface

$$\left. \frac{\partial p_e}{\partial z} \right|_{z=h} = \left. \frac{\partial p_i}{\partial z} \right|_{z=h} = 0 \quad (24)$$

and free flow of liquid at the sample–porous support contact surface

$$p_e|_{z=0} = 0 \quad (25)$$

while the intracellular liquid pressure BC calculation at this surface follows the same logic as with the diffusion problem, giving

$$p_i|_{z=0} = p_{i0} e^{-\frac{\alpha G_{e,i} t}{\mu}}. \quad (26)$$

The solution of Eqs. (16)–(17) under IC and BC Eqs. (22)–(26) is analogous to the one for the diffusion problem, with the sole exceptions

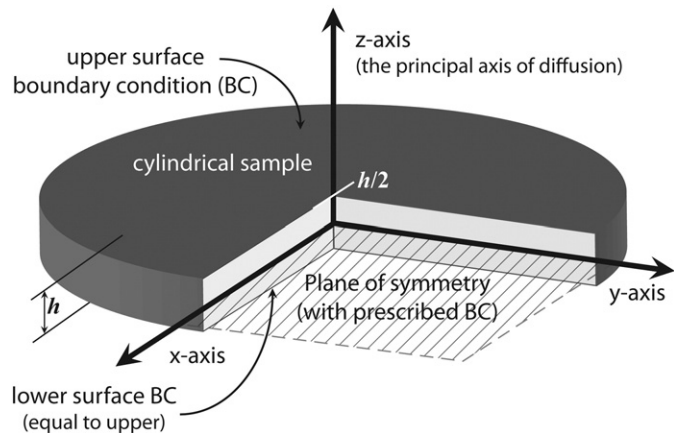


Fig. 4. Schematic representation of the tissue sample as used in the diffusion experiment—the model geometry, coordinate system and boundary conditions (BC).

of sine replacing the cosine in the Fourier series and updating the eigenvalues, due to different boundary conditions (Fig. 5)

$$p_e(z, t) = \frac{4p_{i0}}{\pi} \sum_{n=0}^{\infty} \frac{1}{2n+1} \left((\gamma_{n,1}\tau + 1)C_1 e^{\gamma_{n,1}t} + (\gamma_{n,2}\tau + 1)C_2 e^{\gamma_{n,2}t} \right) \sin\left(\frac{(2n+1)\pi z}{2h}\right) \quad (27)$$

$$p_i(z, t) = \frac{4p_{i0}}{\pi} \sum_{n=0}^{\infty} \frac{1}{2n+1} \left(C_1 e^{\gamma_{n,1}t} + C_2 e^{\gamma_{n,2}t} - e^{-\tau^{-1}t} \right) \sin\left(\frac{(2n+1)\pi z}{2h}\right) + p_{i0} e^{-\tau^{-1}t} \quad (28)$$

where

$$C_1 = \frac{\left(\frac{p_{e0}}{p_{i0}} - 1\right)\tau^{-1} - \gamma_{n,2}}{\gamma_{n,1} - \gamma_{n,2}} \quad (22)$$

$$C_2 = \frac{\left(1 - \frac{p_{e0}}{p_{i0}}\right)\tau^{-1} + \gamma_{n,1}}{\gamma_{n,1} - \gamma_{n,2}} \quad (23)$$

and

$$\gamma_{n,1,2} = \frac{-\left(\tau^{-1}\delta + \lambda_n^2\nu\right) \pm \sqrt{\left(\tau^{-1}\delta + \lambda_n^2\nu\right)^2 - 4\lambda_n^2\nu\tau^{-1}}}{2}. \quad (24)$$

For the sake of algebra, we have set

$$\nu = \frac{k_e G_{e,e}}{\mu}; \quad \tau^{-1} = \frac{\alpha G_{e,i}}{\mu}; \quad \delta = \left(1 + \frac{G_{e,e}}{G_{e,i}}\right) \quad (25)$$

and the eigenvalues λ_n equal $\lambda_n = (2n + 1) \cdot \pi/2h$.

Once liquid pressures are known, we can use Eqs. (18)–(21) to calculate the sample deformation. If we use the dimensionless deformation $s_e(t)$ normalized to the initial sample height, we have

$$s_e(t) = \frac{S_e(t)}{h} = \frac{1}{G_{e,e}} \int_0^1 \int_{p_e(z,t)}^{p_e(z,0)} dp_e \cdot dz + \frac{1}{G_{e,i}} \int_0^1 \int_{p_i(z,t)}^{p_i(z,0)} dp_i \cdot dz. \quad (26)$$

The remaining parameter in need of some explanation is the dimensionless factor α , which accounts for the influence of the electroporation treatment on hydraulic permeability of the cell membrane. According to the theory presented in Mahnič-Kalamiza and Vorobiev (2014), for a spherical cell of radius R , with a stable pore surface fraction f_p consisting of N_p pores of an average radius r_p , it can be written as

$$\alpha = \frac{9f_p r_p^2}{8R^2} \quad (27)$$

where $k_p = r_p^2/8$ is the hydraulic permeability of a single pore.

3. Results and discussion

In this section we present experimental results obtained as described in Sections 2.1–2.3 of the Materials and Methods, the results of model simulations and data fitting, and a discussion on model–experiment correspondence and significance of the necessary alterations in parameter values.

First, we present the dependence of disintegration index Z on the pulse amplitude U (Fig. 6). The bars give standard deviation. Note that the voltage was applied to the electrodes 5 mm apart. Under ideal conditions (homogeneous material, sufficient distance from electrode

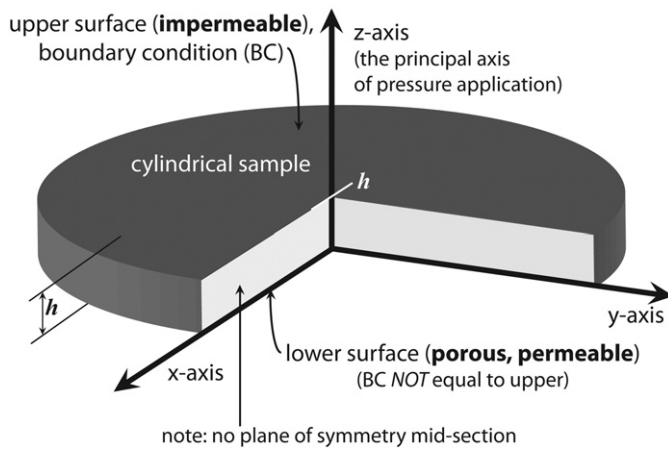


Fig. 5. Schematic representation of the tissue sample as used in the pressing experiment—the model geometry, coordinate system and boundary conditions (BC).

edges), the applied voltage would result in exposure of tissue to a homogeneous electric field of strength $E = U/d$, where U is the voltage applied and d the electrode distance ($d = 5$ mm for all samples in this study). For clarity of presentation, the insert in Fig. 6 gives the dependence for sugar beet tissue only, since the Z response for sugar beet is about an order of a magnitude lower as compared to apple.

We measured Z in order to correlate its dependence on field strength with the subsequent (post-treatment) mass transport. Since we used three different treatment protocols in pressing experiments, we measured Z for apples for all three protocols as well. The conductivity of completely damaged tissue σ_d was determined according to the method described in Section 2.1, and was equal to 20 mS for sugar beet and 10 mS for apple tissue.

The relatively low values of Z can be attributed to the particular treatment protocols used. We chose short treatment times and low voltages that should result in not only irreversible damage to the tissue, but also a significant fraction of reversibly electroporated cells. This is necessary in order to demonstrate the use of the dual-porosity model. If we would have permanently and completely damaged the tissue by irreversible electroporation, we would not have been able to show the influence of the porosity of the electroporated transport-hindering

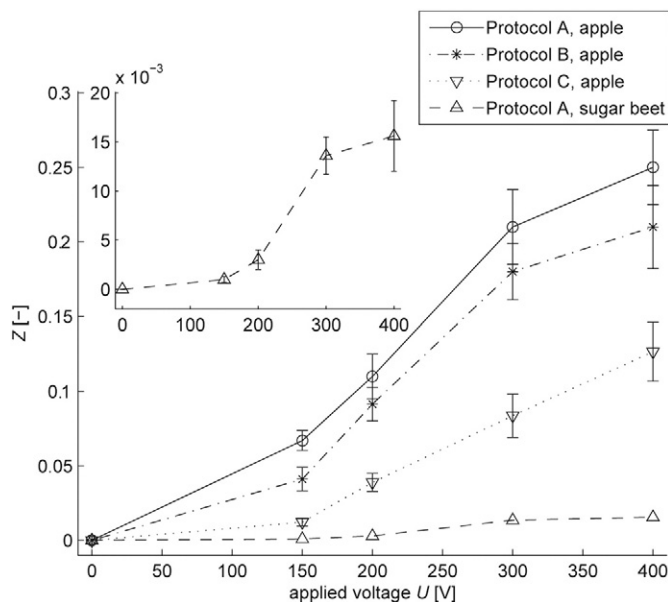


Fig. 6. Disintegration index Z as a function of voltage applied to the electrodes and treatment protocol (the latter for apples only).

membrane. The kinetics of extraction from tissue that has been electroporated to a high degree ($Z \approx 1$) can satisfactorily be represented using a much simpler model of extraction from homogeneous material (Lebovka, Shynkaryk, El-Belghiti, Benjelloun, & Vorobiev, 2007). Treatment protocols used to attain high Z values usually entail the use of hundreds of trains of several pulses or several trains of hundreds of pulses, totaling in treatment times of around 100 ms (Lebovka et al., 2007). In our experiments, the total treatment time never exceeded 1.6 ms.

Use of low-intensity electroporation of biological tissues is not without possible applications in the processing industry. It may open up new possibilities in selective extraction of intracellular compounds, further increasing the purity of juice or extract (Grimi, Praporscic, Lebovka, & Vorobiev, 2007). Or, as in the case of tissue impregnation for e.g. cryopreservation (Shayanfar, Chauhan, Toepfl, & Heinz, 2013), low permanent damage to cells still facilitating molecule uptake (reversible electroporation) is preferred over irreversible damage, as one of the objectives is to preserve the tissue textural properties.

3.1. Diffusion experiments

Fig. 7 gives extraction kinetics obtained in diffusion experiments as described in Materials and Methods (Section 2.2). Experimental data on total solute concentration were fitted with simulated kinetics obtained using the dual-porosity model. Model parameters were optimized to give the best fit to experimental data according to the criterion function, which was the least-square-difference temporal integral. Parameter values are listed in the Appendix, Table A.1, and pore fraction coefficient f_p is additionally given (for convenience) in the legend entries (Fig. 7).

First thing to note comparing Fig. 7a to b, is the comparatively higher yield of soluble solids (predominantly sucrose in sugar beet; and a mixture of sucrose, fructose, and glucose in apple—see e.g. Fuleki et al., 1994) at the end of the 2-h experiment/simulation. In 2 h and given the same applied voltage, more than twice the fractional amount of total solutes detected by the refractometer is extracted from apples as compared to sugar beet. We present two plausible explanations for this difference in final yield: *i*) that cells of apple tissue were permeabilized to a significantly higher degree when same voltage was applied to the electrodes; and/or *ii*) that extracellular space in apples is far more permeable to sugar molecules than in sugar beets. Neglecting the effects of possible differences in membrane composition and electrochemical properties of the liquid medium between the two materials, we suggest three other factors to account for this difference in yield: *i*) larger cells in apple tissue (50 μ m as opposed to 200 μ m in diameter for sugar beets and apples, respectively; Buttersack & Basler, 1991; Harker et al., 2010) result in a higher induced transmembrane voltage, causing more intense permeabilization, which is achieved at lower applied voltage; *ii*) apple tissue is not as compact as sugar beet, the amount of extracellular space is comparatively larger in apples than in sugar beets, leading to a higher rate of diffusion in the extracellular space—note that we suppose the extracellular air is locally replaced by intracellular liquid released from cells at the onset of electroporation or shortly thereafter; and *iii*) the high induced transmembrane voltage on large apple cellular membranes possibly results in irreversible damage to the membranes, thus increasing the intra-to-extracellular space ratio (effectively lowering the cell volume fraction F).

A comparison of extraction kinetics in Fig. 7 and the values of f_p (see Appendix, Table A.2), confirms expectations according to the model and the theory of electroporation; in terms of applied voltage, and significantly higher induced transmembrane voltage due to size difference, we find a lower permeabilization threshold for an average cell in apple tissue as compared to sugar beet. If an average sugar beet cell is much smaller than an average cell in apple tissue, electroporation occurs at correspondingly higher electric field strength, requiring higher applied voltage for a comparable effect. The pore surface fraction (f_p) is on the same order of magnitude at 150 V in apples ($f_p = 0.8 \times 10^{-6}$) as that in sugar beet, but at 300 V ($f_p = 0.9 \times 10^{-6}$). This also indicates that

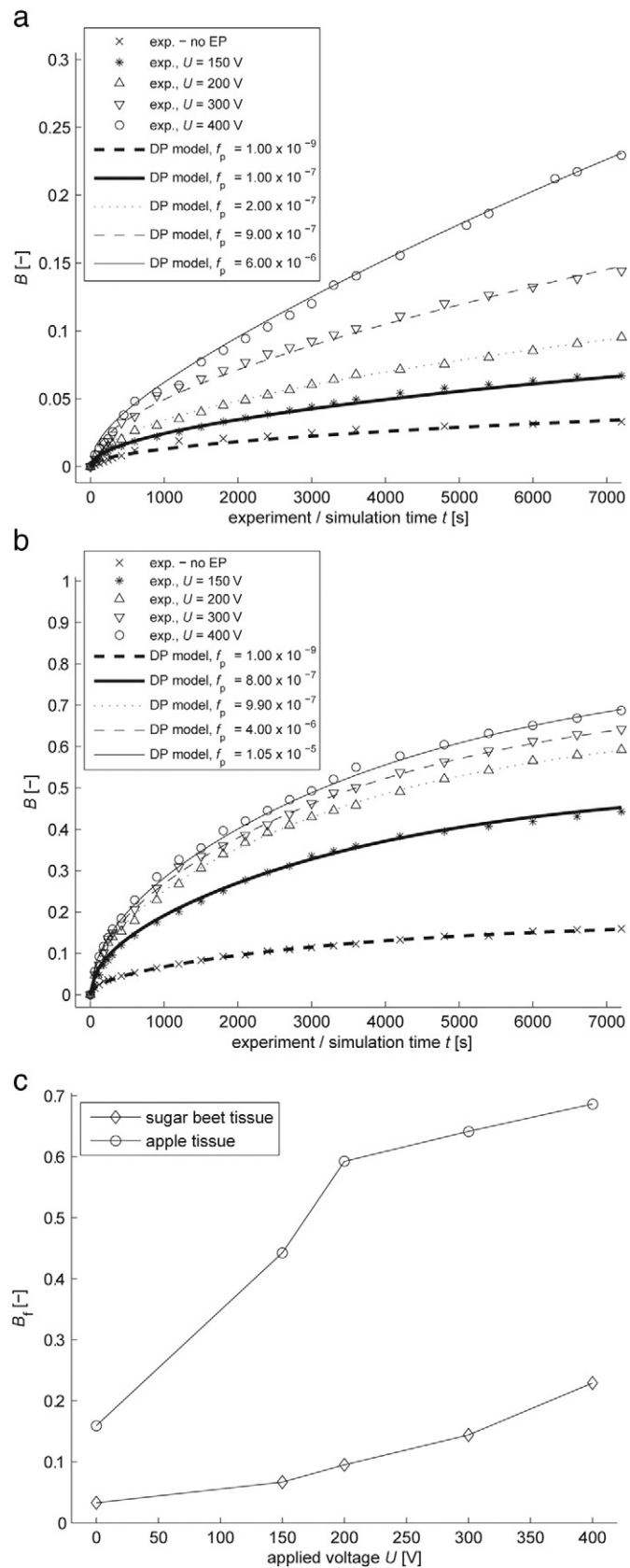


Fig. 7. Results of diffusion experiments (Protocol A) and model simulations of extraction kinetics, for sugar beet (a) and apple (b) tissue. Plot (c) gives the dependence of B_f at the end of the experiment (i.e. B_f) on voltage applied to the electrodes.

we are above the threshold of irreversible electroporation for a large range of cell sizes in apple tissue for voltages above about 200 V, which is reflected in practically insignificant differences in final yield of solutes from apples at 200, 300, and 400 V applied on electrodes (see Fig. 7c).

There are also indications in favor of our assumption that the volume fraction of cells in apple tissue is altered by electroporation due to irreversible damage to cells. We observe the behavior of one of the model parameters (namely F), which needs to vary in order for the simulation to be able to fit the experimental data. Not supposing serious alterations in apple tissue composition (for instance, a decrease in cell volume fraction from initial value of 0.75 for intact apple tissue to 0.265 at 400 V), the model cannot possibly describe the behavior observed in diffusion experiments (the measured yield at the end of the experiment is much too high in comparison to model results, for any value of f_p). This difference cannot be accounted for merely by assuming a higher extracellular diffusion rate (via a strong influence of convective flow for instance), as this would result in simulated extraction kinetics incompatible with experimental data. This reasoning is supported by yet another observation in diffusion kinetics; the kinetics after the first 30 min of experiment exhibits an almost linear behavior in sugar beet, whereas in apples a strong exponential nature of the process is clearly discernible. According to the theory of the dual-porosity model, the behavior as exhibited by apple tissue is expected of a homogeneous material. The lower the volume fraction of cells F , and the higher the fraction of pores on electroporated cells f_p , the more tissue behaves as homogeneous material (i.e. of singular porosity). We can conclude that irreversible electroporation is, from the dual-porosity model point of view, altering tissue composition by rendering cells or domains of cells in tissue into extracellular space, effectively lowering the cell volume fraction in tissue and increasing its bulk porosity.

To conclude the analysis of diffusion experiments, we compare the $Z(U)$ dependence (Fig. 6) with extraction kinetics (Fig. 7a,b). The value of disintegration index Z at 400 V is an order of magnitude lower for sugar beet as compared to apple. However, the resulting extraction yield after 2 h of extraction does not reflect such significant difference. Also, Z measured on apples seems to have an almost linear dependence on applied voltage after the reversible threshold is reached (around 150 V), whereas a clear sigmoid dependence was found for sugar beet tissue. If we compare this with extraction kinetics, we would expect exactly the opposite behavior as is shown in Fig. 7; apple tissue more clearly exhibits a threshold phenomenon, whereas the sucrose yield in sugar beet seems to increase almost linearly between 150 and 300 V applied to the electrodes (see Fig. 7c). In sugar beet, at about 300 V, the reversible field strength threshold of an average cell seems to be reached, and the final sucrose yield increases in disproportion to the increase in applied voltage. Increasing this voltage further above the reversible field strength threshold, we would probably have observed a similar threshold in terms of yield, as we did for apple tissue. To complement these observations, Fig. 8 shows the relationship between the final normalized degree Brix, B_f (total yield at the end of the 2-h experiment/simulation run), and the disintegration index Z . The threshold nature of the electroporation phenomenon is clearly visible; the $B_f(Z)$ linear correlation coefficient for both apple and sugar beet tissue is only around 0.91. Near the critical electric field strength, a small increase in the disintegration index does not reflect in a proportionally small increase in solute yield. The $B_f(Z)$ and $B_f(U)$ dependencies indicate that the reversible field strength threshold of an average sugar beet cell is somewhere above 600 V/cm (note the 5 mm electrode distance), while for apple, the corresponding value is estimated to be just under 300 V/cm. The conclusion is that although Z is a valuable, simple and efficient method of detecting and quantifying tissue electroporation, due to the threshold nature of electroporation, use of Z in predicting aspects of extraction behavior should be carefully (re)examined, at least for protocols resulting in more “gentle” permeabilization (i.e. at low values of Z). Measuring conductivity and

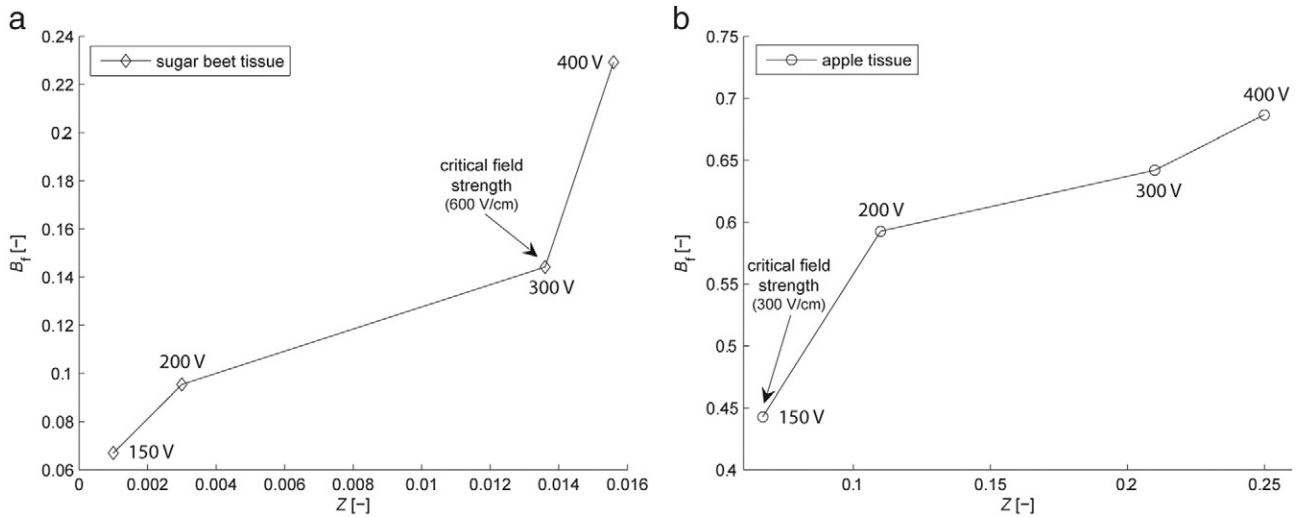


Fig. 8. The $E_f(Z)$ relationship for treatment according to Protocol A; sugar beet (a) and apple (b) tissue. Numbers next to data points indicate the corresponding electrode voltage.

conductivity-based indices are, however, valuable tools in detecting reversible electroporation (Pavlin & Miklavcic, 2008).

3.2. Pressing experiments

Figs. 9 and 10 give pressing kinetics obtained from a texturometer during constant pressure application, as described in Materials and methods (Section 2.3). Experimental data on total tissue sample deformation were fitted with simulation results using the dual-porosity model. Parameters for simulation were optimized to give the best fit with experimental data according to the same criterion function, as was used for the diffusion experiments. Parameter values are listed in the Appendix, Table A.2. Fig. 9 presents extraction kinetics for the two materials as dependent on applied field strength, while Fig. 10 gives expression kinetics for apple tissue using three different protocols (A, B, and C) at three voltages (200, 300, or 400 V).

The pressing experiments further elucidate the behavior of electroporated sample tissues, but more importantly, some of our assumptions about tissue structure and electroporation effects on diffusion can be confirmed by results presented in Fig. 9.

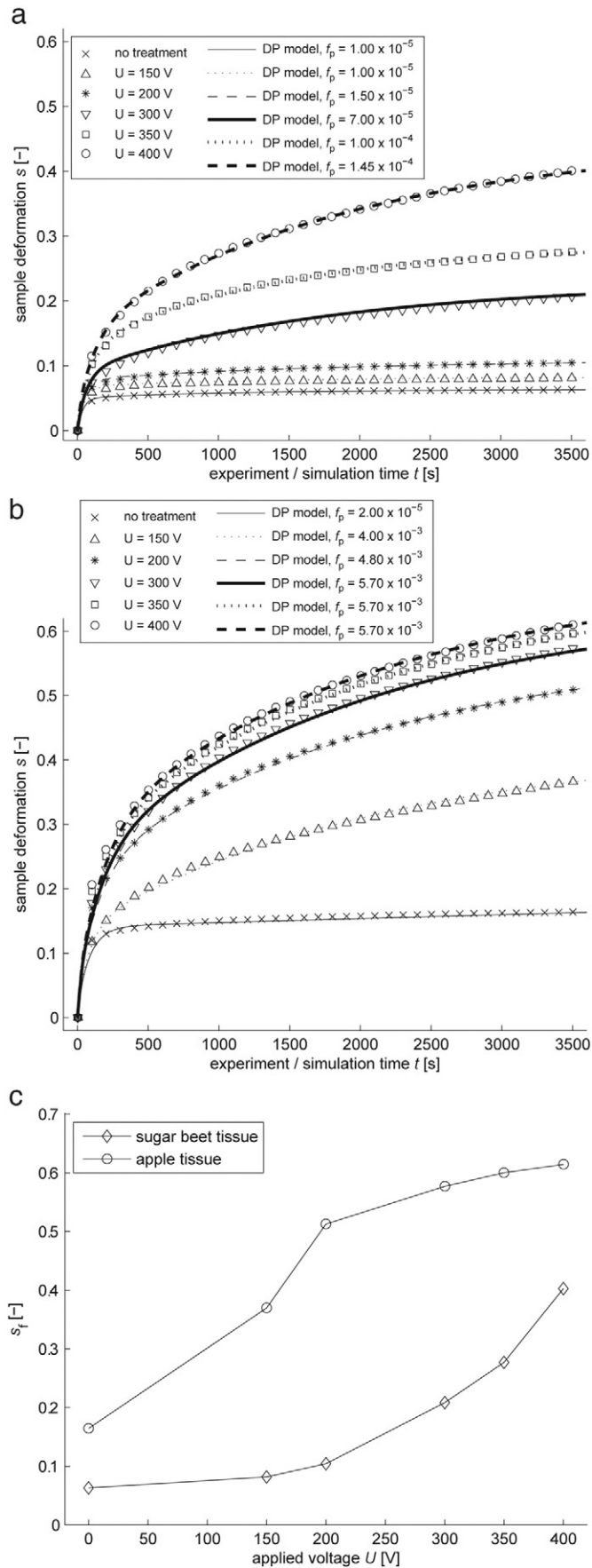
Analogous to the total soluble solutes yield in diffusion experiments, is the total sample deformation at the end of the 1-h pressing experiment. The filtration–consolidation kinetics at 300, 350, and 400 V voltage applied to the 5 mm tissue sample does not differ significantly for apple tissue (see Fig. 9c), while for sugar beet, the final deformation seems to exhibit a roughly quadratic dependence on electric field strength (this dependence was approximately linear in diffusion experiments). This confirms the earlier observation of the lower electroporation threshold for cells in apple tissue. We note that precise cutting and rigorous control via measurements are required to ensure that initial sample thickness is constant in all of the experiments, as an error on the order of 0.5 mm in sample thickness can result in contradictive results (higher final deformation at lower voltage, for example).

Also, the highly compressible extracellular space (about 30% of all sample volume) containing some air and extracellular liquid in intact apple tissue (Fig. 9b), results in a relatively high total sample deformation, as compared to the more densely-packed sugar beet tissue with liquid-filled extracellular space. Note that we did not model the presence of air in the extracellular space of apple tissue; we are assuming that the extracellular air is driven out of the compartments in tissue by intracellular liquid that permeates through the cell membranes at the moment of electroporation or soon thereafter. This can at times be visually observed via appearance of small bubbles of air, provided that a transparent treatment chamber is used and there is enough liquid (juice) around the sample.

Furthermore, final total sample deformation changes most dramatically when applied voltage is increased from 300 to 400 V in sugar beet and from 150 to 200 V in apple tissue (Fig. 9c). This would indicate that, for the pulsing protocols we used, the reversible threshold field strength of an average sugar beet cell is above 600 V/cm, and for the apple this threshold falls somewhere below 300 V/cm (values are estimated based on voltage applied to electrodes over a 5 mm distance). More experiments would be needed for more precise estimates, however, values obtained by analysing pressing experiments are in good agreement with earlier estimates presented in discussion of diffusion data. Also note that using a different treatment protocol (altering the duration and/or number of pulses, temperature, etc.) can result in markedly disparate estimates of the electric field strength required for electroporation, see e.g. (De Vito, Ferrari, Lebovka, Shynkaryk, & Vorobiev, 2008; Lebovka et al., 2007).

A noticeable difference in the consolidation–filtration behavior (apple vs. sugar beet) is caused by the higher extracellular hydraulic permeability of ripe apple. The factor is about 1.5, according to estimates from literature (see Table A.1). However, both the extracellular permeability of apple and of sugar beet tissue had to have been augmented by a factor of 2.5 and 1.5, respectively, in order for the model to successfully fit the experimental extraction kinetics. The extracellular space permeability is potentially a problematic parameter for evaluation; it is time-dependent (it drops in time due to compression of the sample), it cannot be reliably estimated from pressing experiments on intact tissue (only by special, pressure probe or similar experiments), and it is affected by the electroporation treatment as well as a function of ripeness and other biological variables. As discussed in the preceding section on diffusion experiments, electroporation may affect the effective cell volume fraction in tissue, thus reducing hydraulic resistance of tissue, and it may also increase permeability through release of turgor pressure in electroporated cells and consequent plasmolysis (Bazhal, Ngadi, Raghavan, & Nguyen, 2003; Fincan & Dejmeck, 2003; Pereira et al., 2009).

According to the theory of electroporation, higher electric field strength results in a larger area of a cell membrane populated by pores, and thus a larger pore surface fraction per cell (Pavlin & Miklavcic, 2008). For this reason, we modeled electroporation effects on cells in tissue via the parameter f_p —the pore surface fraction. We expect that, given the same treatment conditions and raw material, the pore surface fraction will not depend on whether we are observing diffusion or liquid extraction by pressing. However, comparing values of parameter f_p in Table A.2, we notice a large discrepancy—a difference of about two orders of magnitude in values of f_p when comparing apple tissue in diffusion experiments with pressing experiments. If pore surface fraction is only a function of electroporation parameters (and



according to the theory of electroporation, it is), this observed discrepancy cannot be explained. A possible non-trivial explanation (in the trivial one we conclude that one or more of the model assumptions are wrong) is in the fundamentally different methods of estimation of parameter f_p . Parameter f_p is one of the factors in a coefficient, a product of multiple parameters, which describes the state of membrane permeabilization. In the dual-porosity model equations for diffusion, pore surface fraction is multiplied with the hindrance coefficient, y_s . This parameter relates transmembrane solute diffusion rate with the solute-to-pore size ratio. The relationship is highly non-linear (see Mahnič-Kalamiza et al., 2014). In diffusion experiments with sugar beets or apples, what the pore surface fraction estimate is based on, is the amount of solute detected in the solution outside the tissue sample. The solute is predominantly sucrose (or a mix of sugars), with the hindrance coefficient around 10^{-3} , calculated based on a supposed average and constant pore size. In pressing experiments, the molecules traversing the membrane are not merely sucrose and molecules dissolved in water small enough to pass through the pores, but are primarily the molecules of solvent itself, i.e. intracellular water. Moreover, the hydraulic permeability of the membrane is a product of the pore surface fraction and the assumed constant radius of an average pore. A 10-times larger pore in diameter has a 100-times greater hydraulic permeability. This indirectly implies that in pressing experiments, what we are also measuring is the surface fraction of all pores, those permeable to sugars and those small enough to be permeable to water only. This could also explain why the initial value of f_p for intact tissue, as estimated from pressing experiments, is four orders of magnitude higher than the corresponding value as estimated from diffusion experiments; there are always water-permeable pores, aquaporins (Agre, Sasaki, & Chrispeels, 1993), present in the plasma membrane!

Fig. 10a–c shows the most effective (though not necessarily most energy efficient) treatment protocol for enhancing juice expression from apple tissue is Protocol B, in which only two unipolar pulses 1 s apart of 800 μ s in duration each were applied. The reason for the difference in effectiveness of Protocols A and B might be, as already postulated by De Vito et al., in the longer membrane charging times, required for electroporation of large cells in apple tissue (De Vito et al., 2008). Another possibility is the uncharacterized effect of electrokinetic transport mechanisms (electroosmosis, electrophoresis) that may play a significant role in unipolar pulses on the order of about a millisecond.

Fig. 10a–c also illustrates that Protocol C, with half the total treatment time and carrying between 55–64% (at 400 V) and 78–85% (at 150 V) the energy of Protocols A and B (estimates based on current measurements), is most sensitive to pulse amplitude (also seen in the alternative view, Fig. 10f). Protocol A, by means of which two trains of eight bipolar pulses of 100 μ s each were delivered, shows least sensitivity to pulse amplitude in tissue response (see Fig. 10d). Comparing results in Fig. 10d–f suggests an interesting conclusion; choosing the right treatment protocol (in this case either Protocol A or B, but not C) can at best result in a 40% relative increase (an extra 20% in absolute terms) in juice yield at twice the field strength (400 V as opposed to 200 V)—case of Protocol B. However, doubling the pulse amplitude (and thus, theoretically, at least quadrupling the delivered energy—in practice, the current more than doubles) can have almost negligible effects on juice yield—case of Protocol A. In summary, our results indicate that it is more energy efficient to search for the most appropriate pulsing protocol (depending on material and other treatment and/or processing parameters) and use the lowest sufficiently high voltage, rather than adapt and continue to use a particular protocol that has once proven to be effective and merely increase the voltage until reaching the desired outcome of treatment (e.g. target yield). This observation is of significant

Fig. 9. Results of pressing experiments performed on the texturometer and model simulations of extraction kinetics, with sugar beet (a) and apple (b) tissue. Plot (c) shows the dependence of sample deformation s at the end of the experiment (i.e. s_t) on voltage applied to the electrodes. All samples were electroporated according to Protocol A.

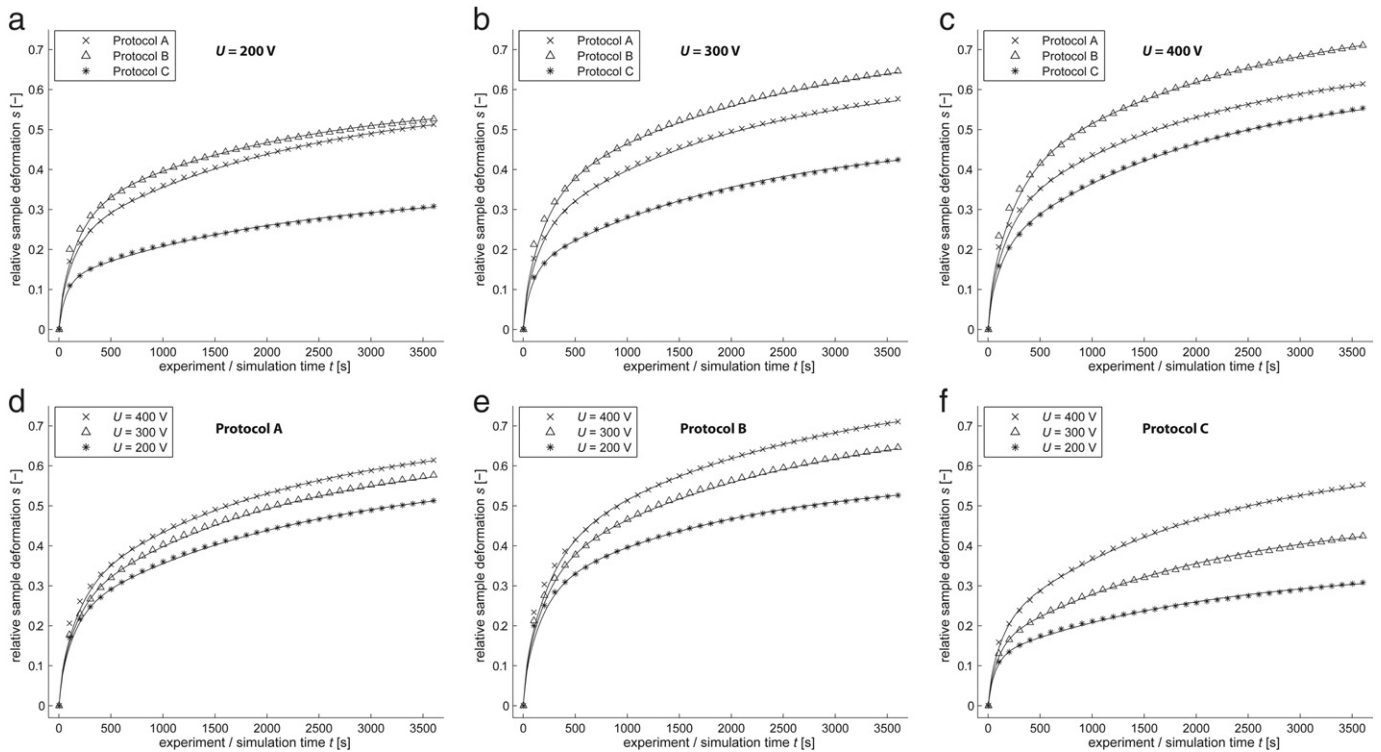


Fig. 10. Protocol comparison at fixed applied voltage during electroporation treatment—results of pressing experiments and model simulations using the dual-porosity model. For clarity, the same results are presented twice—for different voltages applied at the electrodes: 200 V (a), 300 V (b), or 400 V (c); and grouped by one of the three protocols used: Protocol A (d), Protocol B (e), and Protocol C (f).

importance if we consider the transfer from laboratory to industrial scale, as it has implications in operational cost reduction.

Results with Protocol C show that we can also design and apply treatment according to a protocol that exhibits high sensitivity to pulse amplitude. This may be due to significant effects of pore resealing during the second-long pauses between the pulses, as applied according to Protocol C; in other words, the 100 μ s pulses spaced 1 s apart may not be able to stabilise a pore population at lower field strengths. This reasoning is supported by observations in animal cell electroporation (Pucihar, Krmelj, Reberšek, Napotnik, & Miklavčič, 2011). The investigation into various treatment protocols highlights the importance of choosing the optimal parameters of electroporation treatment for achieving extraction efficacy and energy efficiency, at least under conditions of low-energy, “gentle” (low Z) treatment, using few pulses of relatively short duration (on the order of about 10–100 μ s, with total treatment times of 0.1 up to several milliseconds) and low field strengths (under 1 kV/cm).

If we examine the parameters of the dual-porosity model (Appendix, Table A.2) to look for indications of behavior just described, we notice that with the exception of Protocol C, there are no significant deviations from the mean value at the given pulse amplitude. This suggests that pore fraction ratio is indeed, as expected, primarily a function of pulse amplitude. What the protocol parameters seem to influence are the compressibility moduli. From the electroporation theory point of view, we postulate that what the compressibility moduli in some way reflect, are the respective fractions of reversibly and irreversibly electroporated cells. Extracellular space compressibility modulus determines the total relative deformation in the first few seconds to minutes of the pressing experiment. During this first stage, extracellular juice and juice that was or can be released from irreversibly damaged cells is expressed via the extracellular pathways, which are highly permeable. During the second, less dynamic stage, juice is first filtered through the electroporated cell membranes into the extracellular space, as described by the dual-porosity model, and then vacates the tissue sample via the extracellular route. The resulting deformation corresponds to the share of reversibly electroporated cells and is related to the applied pressure via the

intracellular space compressibility modulus. The main difference between Protocol A and Protocol B is found in the values of the compressibility moduli, which indicates that different protocols affect the ratio of (ir)reversibly electroporated cells differently. This is consistent with theory of pore formation and its dependence on local electrochemical material properties. In this respect, Protocol C is particularly interesting; it exhibits the highest ratio of extra-to-intracellular compressibility modulus of all protocols, and the highest sensitivity of pore surface fraction to pulse amplitude, the latter reaching the highest value of all protocols at 400 V pulse amplitude. This is a characteristic of a protocol optimized for achieving reversible electroporation—the ratio of reversibly-to-irreversibly electroporated cells is high (low permanent damage) and reversibly electroporated cells’ membranes are highly permeabilized. Not surprisingly, Protocol C is one of the standard protocols of electrochemotherapy (Lebar, Sersa, Kranjc, Grosej, & Miklavcic, 2002; Mir, Orłowski, Behraderk, & Paoletti, 1991) and gene electrotransfer (Mir et al., 1999), designed for causing minimal lasting damage to tissues and effective reversible electroporation for introducing molecules into target cells.

As the final point, we note the relatively low pressure used for juice expression in our model and experiments. The pressure was either 5.82 bar (sugar beet) or 2.91 bar (apple). This is low in comparison with similar filtration–consolidation behavior studies, where pressures from 1 bar up to 90 bars and higher are used (Grimi, Vorobiev, Lebovka, & Vaxelaire, 2010). This also significantly increased the required experiment duration in our case. We chose low external pressure in order to avoid very important mechanical damage to tissue. If we wish to experimentally observe and model filtration through an electroporated membrane, the integrity of the cell membrane should not be significantly altered due to the applied pressure. We chose the pressure for apple tissue so as to remain well under the saturation limit ($s = 1$) at the end of the 1 h experiment, and though the pressure used for sugar beet could have been further increased according to this saturation criterion, we were limited by the maximum load capabilities of the texturometer.

3.3. Problems, perspectives and directions for future development

The results presented in the preceding sections show that the dual-porosity model can be effectively used to model experimentally-obtained extraction kinetics. There remain, however, several issues that reduce the scientific rigor of the model when applied to practical problems in tissue electroporation. One of these issues concerns treatment parameters in ranges where there may be significant effects to tissue and transport that are not accounted for by the model. This can occur, for instance, under conditions that result in tissue electroporated to a high degree ($Z \approx 1$), or by using a treatment protocol where electrokinetic effects (electroosmosis, electrophoresis) are of significant importance, as these are not captured by the model equations (Li & Lin, 2011b; Li, Tan, Yu, & Lin, 2013a; Movahed & Li, 2012; Sadik, Li, Shan, Shreiber, & Lin, 2013). Electrokinetic effects may already be important under conditions used in this study (up to 800 μs pulses). High degree of electroporation causes problems to modeling of the structure and processes due to irreversible damage to tissue; the model provides parameters that can account for the transition of intracellular to extracellular phase (volume fraction of cells and compressibility moduli), however, as the fraction of irreversibly electroporated cells cannot easily be determined, this unknown variable presents a degree of freedom in the model that influences simulated kinetics much in the same way as the pore surface fraction, the only theoretically determined electroporation-dependent parameter. Recent experiments have shown that future development of the model in the direction of determining reversible/irreversible electroporation thresholds and local damage distribution is unavoidable, as these changes are as important, if not more important, than the permeabilization state of the membrane. In order to model the extent of damage and its distribution, statistical cell size and shape distributions and local inhomogeneities, tissue conductivity and its temporal evolution, and electrokinetic effects will have to be considered. Also, pores resulting from electroporation have a temporal cycle of evolution (e.g. changing size, resealing) that has not been taken into account so far. In conclusion, a more generalized form of the model is required, which entails the need to increase model complexity, and each such expansion or addition must be independently verified, followed by an evaluation of its impact and thus necessity.

Appendix A

Table A.1

Parameters of the dual-porosity model pertaining to tissue textural, geometrical or physicochemical properties, not dependent on electroporation.

Parameter	Sugar beet	Apple	Source (if applicable)
Average cell radius, R [m]	$2.5 \cdot 10^{-5}$	$1.0 \cdot 10^{-4}$	(Buttersack & Basler, 1991; Harker, Redgwell, Hallett, Murray, & Carter, 2010)
Literature-based estimate of cell initial volume fraction, F [-]	0.97	0.75	(Richter & Ehwald, 1983; Vincent, 1989)
Sucrose diffusion constant in water at 20 °C, $D_{s,0}$ [$\text{m}^2 \text{s}^{-1}$]	$4.5 \cdot 10^{-10}$	$4.5 \cdot 10^{-10}$	(Linder, Nassimbeni, Polson, & Rodgers, 1976; Venâncio & Teixeira, 1997)
Extracellular network tortuosity, τ_e [-]	$\pi/2$ (~1.57)	$\pi/2$ (~1.57)	n/a (approximation explained in Mahnič-Kalamiza et al., 2014)
Sucrose-to-pore hydrodynamic radius ratio, r_s/r_p	0.85	0.85	(Mahnič-Kalamiza et al., 2014)
Convection factor, f_c [-] ^a	1	2.5	n/a
Membrane thickness, d_m [m]	$5 \cdot 10^{-9}$	$5 \cdot 10^{-9}$	(Stewart, Gowrishankar, & Weaver, 2004)
Single (average) pore hydraulic permeability, k_p [m^2]	$1.25 \cdot 10^{-19}$	$1.25 \cdot 10^{-19}$	(see Mahnič-Kalamiza & Vorobiev, 2014)
Solvent viscosity, μ [Pa·s]	10^{-3}	10^{-3}	dynamic viscosity of water
Extracellular hydraulic permeability, k_e [m^2]	$1.5 \cdot 10^{-17}$	$2.25 \cdot 10^{-17}$	(Tomos, 1988)
Extracellular hydraulic permeability correction factor, f_k [-] ^b	1.5	2.5	n/a
Spherical cell squared surface-to-volume ratio (for α), $9/R^2$ [m^{-2}]	$1.44 \cdot 10^{10}$	$9.00 \cdot 10^8$	n/a
Applied (via piston) external pressure, P_E [MPa]	0.582 (5.82 bar)	0.291 (2.91 bar)	n/a

^a The convection factor augments the extracellular diffusion rate ($D_{s,e} = D_{s,e} / \tau_e \cdot f_c$) to account for the effect of convection (washing out) of solute from the tissue samples due to solvent agitation. It was computationally determined based on comparison of model predictions and experimentally observed kinetics of solute percolating through the tissue matrix out of samples into the solvent. The effect was observed in apple tissue but not in sugar beets. The reason for this may be the relatively low packing ratio (cell-to-cell contacts, void extracellular space) of apple tissue (Harker et al., 2010). In part, the faster rate of diffusion can also be attributed to sugar composition in apple fruits; compared to sugar beet taproots, there are significant amounts of fructose and glucose present, molecules which are smaller than sucrose and with higher diffusion coefficients (Fuleki, Pelayo, & Palabay, 1994; Venâncio & Teixeira, 1997).

^b In both sugar beet and apple tissue, the estimated extracellular space hydraulic permeability recalculated from measurements reported in literature had to have been augmented by a certain factor to account for experimentally-observed faster expression rate as opposed to the rate governed by the estimated permeability coefficient. This is most likely due to the fact the effect of electrical treatment on extracellular permeability (particularly noticeable in apple tissue) is not accounted for in the model equations.

4. Conclusions

In our previous papers we set out to describe a new framework for studying mass transport in electroporated tissue—i.e. the dual-porosity model of solute diffusion and consolidation–filtration behavior of electroporated tissue. In this paper we describe experiments on two model materials, sugar beet taproot and apple fruit tissue, which we used to test the model performance and verify some of the basic model assumptions. We have demonstrated the model is capable of accurately modeling extraction kinetics obtained by diffusion as well as pressing experiments. During model construction, we have identified and chose one model parameter, the pore surface fraction, as the most important parameter that is a function of electroporation treatment parameters—the local electric field strength, pulse number, and pulse duration. In this work, we have identified other important factors (most importantly changes in permeability and compressibility of tissue due to structural modifications) that reflect the complicated nature of electric field effects on texture and mass transport in electroporated tissue. To develop the model further, we need to evaluate their influence and mathematically describe these effects, to arrive at a more generalized model solution, capable of predicting extraction kinetics based on treatment parameters and material characteristics that can be obtained either from literature or estimated by independent experiments. We are confident the model can already be successfully applied to evaluate electroporation treatment efficiency with respect to mass transport, that it can be used for optimization of treatment parameters with prediction of treatment results, and that its further development will help understand the phenomena related to mass transport and textural properties of electroporated biological material.

Acknowledgments

The authors appreciate the financial support from the French Ministry of Research and Higher Education and the Slovenian Research Agency. This research was in part made possible due to networking activity of COST TD1104 Action (www.electroporation.net). We (SMK and DM) would also like to thank Dr. Sid Becker from the University of Canterbury, New Zealand, for fruitful discussion on the theory of porous media as applied to problems in tissue electroporation.

Table A.2

Parameters of the dual-porosity model with dependence on electroporation treatment used to fit experimental data in diffusion (shown in Fig. 7) and pressing experiments (as shown in Figs. 9 and 10).

Tissue	U [V]	Diffusion experiments			Pressing experiments		
		f_p [-]	C_{e0}/C_{i0} [-]	F [-]	f_p [-]	$\bar{C}_{e,e}$ [Pa]	$\bar{C}_{e,i}$ [Pa]
Sugar beet	0	$1.0 \cdot 10^{-9}$	0.65	0.92	$1.00 \cdot 10^{-5}$	$115.0 \cdot 10^5$	$450.0 \cdot 10^5$
	150	$1.0 \cdot 10^{-7}$	1.00	0.90	$1.00 \cdot 10^{-5}$	$85.0 \cdot 10^5$	$400.0 \cdot 10^5$
	200	$2.0 \cdot 10^{-7}$	1.00	0.86	$1.50 \cdot 10^{-5}$	$73.0 \cdot 10^5$	$200.0 \cdot 10^5$
	300	$9.0 \cdot 10^{-7}$	1.00	0.80	$7.00 \cdot 10^{-5}$	$58.0 \cdot 10^5$	$45.0 \cdot 10^5$
	350	n/a	n/a	n/a	$1.00 \cdot 10^{-4}$	$39.5 \cdot 10^5$	$41.5 \cdot 10^5$
Apple (Protocol A)	400	$6.0 \cdot 10^{-6}$	1.00	0.77	$1.45 \cdot 10^{-4}$	$32.0 \cdot 10^5$	$22.0 \cdot 10^5$
	0	$1.0 \cdot 10^{-9}$	0.65	0.75	$2.00 \cdot 10^{-5}$	$20.5 \cdot 10^5$	$12.0 \cdot 10^5$
	150	$8.0 \cdot 10^{-7}$	1.00	0.50	$4.00 \cdot 10^{-3}$	$18.5 \cdot 10^5$	$11.0 \cdot 10^5$
	200	$9.9 \cdot 10^{-7}$	1.00	0.345	$4.80 \cdot 10^{-3}$	$11.0 \cdot 10^5$	$9.2 \cdot 10^5$
	300	$4.0 \cdot 10^{-6}$	1.00	0.30	$5.70 \cdot 10^{-3}$	$9.80 \cdot 10^5$	$8.5 \cdot 10^5$
Apple (Protocol B)	350	n/a	n/a	n/a	$5.70 \cdot 10^{-3}$	$9.00 \cdot 10^5$	$8.45 \cdot 10^5$
	400	$1.05 \cdot 10^{-5}$	1.00	0.265	$5.70 \cdot 10^{-3}$	$8.60 \cdot 10^5$	$8.45 \cdot 10^5$
	200	n/a			$4.20 \cdot 10^{-3}$	$9.00 \cdot 10^5$	$11.6 \cdot 10^5$
	300				$4.85 \cdot 10^{-3}$	$7.50 \cdot 10^5$	$8.5 \cdot 10^5$
Apple (Protocol C)	400				$5.10 \cdot 10^{-3}$	$6.55 \cdot 10^5$	$8.0 \cdot 10^5$
	200	n/a			$3.20 \cdot 10^{-3}$	$21.2 \cdot 10^5$	$14.0 \cdot 10^5$
	300				$4.80 \cdot 10^{-3}$	$16.3 \cdot 10^5$	$9.6 \cdot 10^5$
	400				$6.35 \cdot 10^{-3}$	$11.8 \cdot 10^5$	$7.8 \cdot 10^5$

References

- Agre, P., Sasaki, S., & Chrispeels, M.J. (1993). Aquaporins: A family of water channel proteins. *American Journal of Physiology - Renal Physiology*, 265(3), F461.
- Ariffin, A.B., Forde, P.F., Jahangeer, S., Soden, D.M., & Hinchion, J. (2014). Releasing pressure in tumors: What do we know so far and where do we go from here? A review. *Cancer Research*, 74(10), 2655–2662. <http://dx.doi.org/10.1158/0008-5472.CAN-13-3696>.
- Bazhal, M.I., Ngadi, M.O., Raghavan, G.S.V., & Nguyen, D.H. (2003). Textural changes in apple tissue during pulsed electric field treatment. *Journal of Food Science*, 68(1), 249–253. <http://dx.doi.org/10.1111/j.1365-2621.2003.tb14147.x>.
- Becker, S. (2012). Transport modeling of skin electroporation and the thermal behavior of the stratum corneum. *International Journal of Thermal Sciences*, 54, 48–61. <http://dx.doi.org/10.1016/j.ijthermalsci.2011.10.022>.
- Boussetta, N., Soichi, E., Lanoiselle, J.-L., & Vorobiev, E. (2014). Valorization of oilseed residues: Extraction of polyphenols from flaxseed hulls by pulsed electric fields. *Industrial Crops and Products*, 52, 347–353. <http://dx.doi.org/10.1016/j.indcrop.2013.10.048>.
- Buttersack, C., & Basler, W. (1991). Hydraulic conductivity of cell-walls in sugar-beet tissue. *Plant Science*, 76(2), 229–237. [http://dx.doi.org/10.1016/0168-9452\(91\)90145-X](http://dx.doi.org/10.1016/0168-9452(91)90145-X).
- Cadossi, R., Ronchetti, M., & Cadossi, M. (2014). Locally enhanced chemotherapy by electroporation: Clinical experiences and perspective of use of electrochemotherapy. *Future Oncology (London, England)*, 10(5), 877–890. <http://dx.doi.org/10.2217/fon.13.235>.
- Campbell, N.A., Reece, J.B., Urry, L.A., Cain, M.L., Wasserman, S.A., Minorsky, P.V., et al. (2008). *Biology*. San Francisco: Pearson, Benjamin Cummings.
- De Monte, F., Pontrelli, G., & Becker, S. (2013). Chapter 3—Drug release in biological tissues. In S.M. Becker, & A.V. Kuznetsov (Eds.), *Transport in biological media* (pp. 59–118). Boston: Elsevier (Retrieved from <http://www.sciencedirect.com/science/article/pii/B9780124158245000035>).
- De Vito, F., Ferrari, G., Lebovka, N.I., Shynkaryk, N.V., & Vorobiev, E. (2008). Pulse duration and efficiency of soft cellular tissue disintegration by pulsed electric fields. *Food and Bioprocess Technology*, 1(4), 307–313. <http://dx.doi.org/10.1007/s11947-007-0017-y>.
- Dean, D.A. (2013). Cell-specific targeting strategies for electroporation-mediated gene delivery in cells and animals. *Journal of Membrane Biology*, 246(10), 737–744. <http://dx.doi.org/10.1007/s00232-013-9534-y>.
- Donsi, F., Ferrari, G., & Pataro, G. (2010). Applications of pulsed electric field treatments for the enhancement of mass transfer from vegetable tissue. *Food Engineering Reviews*, 2(2), 109–130. <http://dx.doi.org/10.1007/s12393-010-9015-3>.
- El Belghiti, K.E., & Vorobiev, E. (2004). Mass transfer of sugar from beets enhanced by pulsed electric field. *Food and Bioprocess Technology*, 82(C3), 226–230.
- Fincan, M., & Dejmek, P. (2003). Effect of osmotic pretreatment and pulsed electric field on the viscoelastic properties of potato tissue. *Journal of Food Engineering*, 59(2–3), 169–175. [http://dx.doi.org/10.1016/S0260-8774\(02\)00454-5](http://dx.doi.org/10.1016/S0260-8774(02)00454-5).
- Fuleki, T., Pelayo, E., & Palabay, R.B. (1994). Sugar composition of varietal juices produced from fresh and stored apples. *Journal of Agricultural and Food Chemistry*, 42(6), 1266–1275. <http://dx.doi.org/10.1021/jf00042a003>.
- Gehl, J. (2003). Electroporation: Theory and methods, perspectives for drug delivery, gene therapy and research. *Acta Physiologica Scandinavica*, 177(4), 437–447. <http://dx.doi.org/10.1046/j.1365-201X.2003.01093.x>.
- Goettl, M., Eing, C., Gusbeth, C., Straessner, R., & Frey, W. (2013). Pulsed electric field assisted extraction of intracellular valuable from microalgae. *Algal Research - Biomass Biofuels and Bioproducts*, 2(4), 401–408. <http://dx.doi.org/10.1016/j.algal.2013.07.004>.
- Golberg, A., & Yarmush, M.L. (2013). Nonthermal irreversible electroporation: Fundamentals, applications, and challenges. *IEEE Transactions on Biomedical Engineering*, 60(3), 707–714. <http://dx.doi.org/10.1109/TBME.2013.2238672>.
- Grimi, N., Dubois, A., Marchal, L., Jubeau, S., Lebovka, N.I., & Vorobiev, E. (2014). Selective extraction from microalgae *Nannochloropsis* sp. using different methods of cell disruption. *Bioresource Technology*, 153, 254–259. <http://dx.doi.org/10.1016/j.biortech.2013.12.011>.
- Grimi, N., Praporscic, I., Lebovka, N., & Vorobiev, E. (2007). Selective extraction from carrot slices by pressing and washing enhanced by pulsed electric fields. *Separation and Purification Technology*, 58(2), 267–273. <http://dx.doi.org/10.1016/j.seppur.2007.03.020>.
- Grimi, N., Vorobiev, E., Lebovka, N., & Vaxelaire, J. (2010). Solid–liquid expression from denaturated plant tissue: Filtration–consolidation behaviour. *Journal of Food Engineering*, 96(1), 29–36. <http://dx.doi.org/10.1016/j.jfoodeng.2009.06.039>.
- Haberl, S., Miklavcic, D., Sersa, G., Frey, W., & Rubinsky, B. (2013). Cell membrane electroporation-Part 2: The applications. *IEEE Electrical Insulation Magazine*, 29(1), 29–37.
- Harker, F.R., Redgwell, R.J., Hallett, I.C., Murray, S.H., & Carter, G. (2010). Texture of fresh fruit. In J. Janick (Ed.), *Horticultural reviews* (pp. 121–224). John Wiley & Sons, Inc (Retrieved from <http://onlinelibrary.wiley.com/doi/10.1002/9780470650646.ch2/summary>).
- Jiang, C., Qin, Z., & Bischof, J. (2014). Membrane-targeting approaches for enhanced cancer cell destruction with irreversible electroporation. *Annals of Biomedical Engineering*, 42(1), 193–204. <http://dx.doi.org/10.1007/s10439-013-0882-7>.
- Kotnik, T., Kramar, P., Pucihar, G., Miklavcic, D., & Tarek, M. (2012). Cell membrane electroporation-Part 1: The phenomenon. *IEEE Electrical Insulation Magazine*, 28(5), 14–23. <http://dx.doi.org/10.1109/MEI.2012.6268438>.
- Lebar, A.M., Sersa, G., Kranjc, S., Grosej, A., & Miklavcic, D. (2002). Optimisation of pulse parameters in vitro for in vivo electrochemotherapy. *Anticancer Research*, 22(3), 1731–1736.
- Lebovka, N.I., Shynkaryk, M.V., El-Belghiti, K., Benjelloun, H., & Vorobiev, E. (2007). Plasmolysis of sugarbeet: Pulsed electric fields and thermal treatment. *Journal of Food Engineering*, 80(2), 639–644. <http://dx.doi.org/10.1016/j.jfoodeng.2006.06.020>.
- Li, J., & Lin, H. (2011a). Numerical simulation of molecular uptake via electroporation. *Bioelectrochemistry*, 82(1), 10–21. <http://dx.doi.org/10.1016/j.bioelechem.2011.04.006>.
- Li, J., & Lin, H. (2011b). Numerical simulation of molecular uptake via electroporation. *Bioelectrochemistry (Amsterdam, Netherlands)*, 82(1), 10–21. <http://dx.doi.org/10.1016/j.bioelechem.2011.04.006>.
- Li, J., Tan, W., Yu, M., & Lin, H. (2013a). The effect of extracellular conductivity on electroporation-mediated molecular delivery. *Biochimica et Biophysica Acta*, 1828(2), 461–470. <http://dx.doi.org/10.1016/j.bbame.2012.08.014>.
- Li, J., Tan, W., Yu, M., & Lin, H. (2013b). The effect of extracellular conductivity on electroporation-mediated molecular delivery. *Biochimica et Biophysica Acta*, 1828(2), 461–470. <http://dx.doi.org/10.1016/j.bbame.2012.08.014>.
- Linder, P.W., Nassimbeni, L.R., Polson, A., & Rodgers, A.L. (1976). The diffusion coefficient of sucrose in water. A physical chemistry experiment. *Journal of Chemical Education*, 53(5), 330. <http://dx.doi.org/10.1021/ed053p330>.
- Liu, L.J., Brown, S.L., Ewing, J.R., & Schlesinger, M. (2011). Phenomenological model of interstitial fluid pressure in a solid tumor. *Physical Review E: Statistical, Nonlinear, and Soft Matter Physics*, 84(2 Pt 1), 021919.
- Liu, D., Lebovka, N.I., & Vorobiev, E. (2013). Impact of electric pulse treatment on selective extraction of intracellular compounds from *Saccharomyces cerevisiae* yeasts. *Food and Bioprocess Technology*, 6(2), 576–584. <http://dx.doi.org/10.1007/s11947-011-0703-7>.
- Mahnič-Kalamiza, S., Miklavcic, D., & Vorobiev, E. (2014). Dual-porosity model of solute diffusion in biological tissue modified by electroporation. *Biochimica et Biophysica Acta*, 1838(7), 1950–1966. <http://dx.doi.org/10.1016/j.bbame.2014.03.004>.

- Mahnič-Kalamiza, S., & Vorobiev, E. (2014). Dual-porosity model of liquid extraction by pressing from biological tissue modified by electroporation. *Journal of Food Engineering*, 137, 76–87. <http://dx.doi.org/10.1016/j.jfoodeng.2014.03.035>.
- Marty, M., Sersa, G., Garbay, J.R., Gehl, J., Collins, C.G., Snoj, M., et al. (2006). Electrochemotherapy—An easy, highly effective and safe treatment of cutaneous and subcutaneous metastases: Results of ESOPE (European Standard Operating Procedures of Electrochemotherapy) study. *European Journal of Cancer Supplements*, 4(11), 3–13. <http://dx.doi.org/10.1016/j.ejcsup.2006.08.002>.
- Miklavcic, D., Mali, B., Kos, B., Heller, R., & Sersa, G. (2014). Electrochemotherapy: From the drawing board into medical practice. *Biomedical Engineering Online*, 13, 29. <http://dx.doi.org/10.1186/1475-925X-13-29>.
- Mir, L.M., Bureau, M.F., Gehl, J., Rangara, R., Rouy, D., Caillaud, J.-M., et al. (1999). High-efficiency gene transfer into skeletal muscle mediated by electric pulses. *Proceedings of the National Academy of Sciences of the United States of America*, 96(8), 4262–4267.
- Mir, L.M., Orłowski, S., Belehradec, J., Jr., & Paoletti, C. (1991). Electrochemotherapy potentiation of antitumour effect of bleomycin by local electric pulses. *European Journal of Cancer (Oxford, England : 1990)*, 27(1), 68–72.
- Morales-de la Pena, M., Elez-Martinez, P., & Martin-Belloso, O. (2011). Food preservation by pulsed electric fields: An engineering perspective. *Food Engineering Reviews*, 3(2), 94–107. <http://dx.doi.org/10.1007/s12393-011-9035-7>.
- Movahed, S., & Li, D. (2012). Electrokinetic transport through the nanopores in cell membrane during electroporation. *Journal of Colloid and Interface Science*, 369, 442–452. <http://dx.doi.org/10.1016/j.jcis.2011.12.039>.
- Mykhailiyk, V., & Lebovka, N. (2014). Specific heat of apple at different moisture contents and temperatures. *Journal of Food Engineering*, 123, 32–35. <http://dx.doi.org/10.1016/j.jfoodeng.2013.09.015>.
- Pavlin, M., & Miklavcic, D. (2008). Theoretical and experimental analysis of conductivity, ion diffusion and molecular transport during cell electroporation - Relation between short-lived and long-lived pores. *Bioelectrochemistry*, 74(1), 38–46. <http://dx.doi.org/10.1016/j.bioelechem.2008.04.016>.
- Pereira, R.N., Galindo, F.G., Vicente, A.A., & Dejmeek, P. (2009). Effects of pulsed electric field on the viscoelastic properties of potato tissue. *Food Biophysics*, 4(3), 229–239. <http://dx.doi.org/10.1007/s11483-009-9120-0>.
- Petryk, M., & Vorobiev, E. (2013). Numerical and analytical modeling of solid-liquid expression from soft plant materials. *AIChE Journal*, 59(12), 4762–4771. <http://dx.doi.org/10.1002/aic.14213>.
- Pucihar, G., Kotnik, T., Miklavcic, D., & Teissie, J. (2008). Kinetics of transmembrane transport of small molecules into electroporabilized cells. *Biophysical Journal*, 95(6), 2837–2848. <http://dx.doi.org/10.1529/biophysj.108.135541>.
- Pucihar, G., Krmelj, J., Reberšek, M., Napotnik, T.B., & Miklavčič, D. (2011). Equivalent pulse parameters for electroporation. *IEEE Transactions on Biomedical Engineering*, 58(11), 3279–3288. <http://dx.doi.org/10.1109/TBME.2011.2167232>.
- Pusenjak, J., & Miklavcic, D. (2000). Modeling of interstitial fluid pressure in solid tumor. *Simulation Practice and Theory*, 8(1–2), 17–24. [http://dx.doi.org/10.1016/S0928-4869\(00\)00003-3](http://dx.doi.org/10.1016/S0928-4869(00)00003-3).
- Raso, J., & Heinz, V. (2010). *Pulsed electric fields technology for the food industry: Fundamentals and applications*. Springer.
- Reigada, R. (2014). Electroporation of heterogeneous lipid membranes. *Biochimica Et Biophysica Acta - Biomembranes*, 1838(3), 814–821. <http://dx.doi.org/10.1016/j.bbmem.2013.10.008>.
- Richter, E., & Ehwald, R. (1983). Apoplastic mobility of sucrose in storage parenchyma of sugar beet. *Physiologia Plantarum*, 58(3), 263–268. <http://dx.doi.org/10.1111/j.1399-3054.1983.tb04179.x>.
- Sadik, M.M., Li, J., Shan, J.W., Shreiber, D.I., & Lin, H. (2013). Quantification of propidium iodide delivery using millisecond electric pulses: Experiments. *Biochimica et Biophysica Acta*, 1828(4), 1322–1328. <http://dx.doi.org/10.1016/j.bbmem.2013.01.002>.
- Saulis, G. (2010). Electroporation of cell membranes: The fundamental effects of pulsed electric fields in food processing. *Food Engineering Reviews*, 2(2), 52–73. <http://dx.doi.org/10.1007/s12393-010-9023-3>.
- Sel, D., Cukjati, D., Batuskaite, D., Slivnik, T., Mir, L.M., & Miklavcic, D. (2005). Sequential finite element model of tissue electroporation. *IEEE Transactions on Biomedical Engineering*, 52(5), 816–827. <http://dx.doi.org/10.1109/TBME.2005.845212>.
- Shayanfar, S., Chauhan, O.P., Toepfl, S., & Heinz, V. (2013). The interaction of pulsed electric fields and texturizing - antifreezing agents in quality retention of defrosted potato strips. *International Journal of Food Science and Technology*, 48(6), 1289–1295. <http://dx.doi.org/10.1111/ijfs.12089>.
- Simonsen, T.G., Gaustad, J. -V., Leinaas, M.N., & Rofstad, E.K. (2012). High interstitial fluid pressure is associated with tumor-line specific vascular abnormalities in human melanoma xenografts. *PLoS One*, 7(6), e40006. <http://dx.doi.org/10.1371/journal.pone.0040006>.
- Sridhara, V., & Joshi, R.P. (2014). Evaluations of a mechanistic hypothesis for the influence of extracellular ions on electroporation due to high-intensity, nanosecond pulsing. *Biochimica et Biophysica Acta*, 1838(7), 1793–1800. <http://dx.doi.org/10.1016/j.bbmem.2014.03.010>.
- Stewart, D.A., Gowrishankar, I.R., & Weaver, J.C. (2004). Transport lattice approach to describing cell electroporation: Use of a local asymptotic model. *IEEE Transactions on Plasma Science*, 32(4), 1696–1708. <http://dx.doi.org/10.1109/TPS.2004.832639>.
- Tomos, A.D. (1988). Cellular water relations of plants. In F. Franks (Ed.), *Water Science Reviews 3 (1st ed.)*. Water dynamics. Cambridge University Press (Vol.).
- Turk, M.F., Vorobiev, E., & Baron, A. (2012). Improving apple juice expression and quality by pulsed electric field on an industrial scale. *LWT - Food Science and Technology*, 49(2), 245–250. <http://dx.doi.org/10.1016/j.lwt.2012.07.024>.
- Venâncio, A., & Teixeira, J.A. (1997). Characterization of sugar diffusion coefficients in alginate membranes. *Biotechnology Techniques*, 11(3), 183–186. <http://dx.doi.org/10.1023/A:1018457631368>.
- Vincent, J.F.V. (1989). Relationship between density and stiffness of apple flesh. *Journal of the Science of Food and Agriculture*, 47(4), 443–462. <http://dx.doi.org/10.1002/jsfa.1740470406>.
- Vorobiev, E., & Lebovka, N. (2008). Pulsed-electric-fields-induced effects in plant tissues: Fundamental aspects and perspectives of applications. *Electrotechnologies for extraction from food plants and biomaterials* (pp. 39–81). New York: Springer (Retrieved from http://link.springer.com/chapter/10.1007/978-0-387-79374-0_2).
- Yarmush, M.L., Golberg, A., Serša, G., Kotnik, T., & Miklavčič, D. (2014). Electroporation-based technologies for medicine: Principles, applications, and challenges. *Annual Review of Biomedical Engineering*, 16(1), 295–320. <http://dx.doi.org/10.1146/annurev-bioeng-071813-104622>.
- Zorec, B., Préat, V., Miklavčič, D., & Pavšelj, N. (2013). Active enhancement methods for intra- and transdermal drug delivery: A review. *Slovenian Medical Journal*, 82(5). <http://dx.doi.org/10.6016/1889>.